TecnoLógicas

Behavior of Composite Piles Subjected to Combined Loads: Numerical Analysis

Comportamiento de pilotes compuestos sometidos a cargas combinadas: análisis numérico

Alejandro Nasner-Caipe[1]; Carlos Alberto Vega-Posada[1,2]; Edwin García-Aristizábal[1]

[1]Universidad de Antioquia – UdeA, Facultad de Ingeniería, Escuela Ambiental, Medellín-Colombia.
[2]Universidad Nacional de Colombia, Dept. de Ingeniería Civil, Medellín-Colombia.

Correspondence: alejandro.nasner@udea.edu.co

Received: 21 November 2025 **Accepted:** 26 August 2026 **Available:** 03 September 2026

How to cite / Cómo citar

A. Nasner-Caipe, C. A. Vega-Posada, and E. García-Aristizábal, "Behavior of Composite Piles Subjected to Combined Loads: Numerical Analysis," *TecnoLógicas*, vol. 29, no. 67, e3769, 2026.
https://doi.org/10.22430/22565337.3769

CC BY NC SA

Abstract

Piles are one-dimensional (1D) beam–column elements designed to support axial loads from superstructures. However, in tall buildings, ports, bridges, and both onshore and offshore structures, they are subjected to combined loads that include axial forces, lateral loads, and bending moments. The study of pile behavior under such loading remains limited, particularly in the numerical evaluation of the combined effects of composite geometry and soil stratification. At the same time, analysis and design are based primarily on Timoshenko (TB) and Euler–Bernoulli (EBB) beam theories. The objective of this research was to numerically assess the behavior of composite piles under combined loads. Three cases were considered: i) a homogeneous soil layer, ii) stratified two-layer soils, and iii) composite sections, to analyze the influence of such loads on structural response and soil–structure interaction. The methodology included incremental static analyzes under axial and lateral loads using SAP2000 finite element software. Three numerical examples were developed to evaluate the performance of embedded Concrete-Filled Steel Tubular Piles (CFSTP) with circular and square cross sections. The results revealed two trends depending on the axial load: $0 < P \leq 5$ MN and $P > 5$ MN. Regardless of the soil stiffness ratio ($k_{s1}/k_{s2} = 0.5–1.5$), the lateral performance was dominated by geometry, the square–square pile (SSP) being the most efficient, followed by the circular–circular pile (CCP) and the solid pile (SP). The maximum bending moments were slightly higher in the stiffer sections, particularly in SSP and CCP. Finally, it is concluded that the axial load induces a dual effect: it amplifies lateral deflections while reducing the variation in bending moment, demonstrating that cross-sectional geometry is the dominant parameter in pile performance.

Keywords

Combined loads, composite pile foundations, lateral response, numerical modeling, soil–structure interaction.

Resumen

Los pilotes son elementos viga–columna unidimensionales (1D) diseñados para soportar cargas axiales de la superestructura. Sin embargo, en edificios altos, puertos, puentes y estructuras terrestres y marinas, están sometidos a cargas combinadas que incluyen fuerzas axiales, cargas laterales y momentos flectores. El estudio del comportamiento de pilotes bajo estas solicitaciones sigue siendo limitado, particularmente en la evaluación numérica de los efectos combinados de la geometría compuesta y la estratificación del suelo, mientras que su análisis y diseño se basan principalmente en las teorías de viga de Timoshenko (TB) y Euler–Bernoulli (EBB). El objetivo de esta investigación fue evaluar mediante análisis numérico el comportamiento de pilotes compuestos sometidos a cargas combinadas. Para analizar la influencia de dichas cargas en la respuesta estructural y la interacción suelo–estructura se consideraron: i) un estrato homogéneo, ii) suelos estratificados en dos capas y iii) secciones compuestas. La metodología incluyó análisis estáticos incrementales bajo cargas axiales y laterales mediante el software de elementos finitos SAP2000. Se desarrollaron tres ejemplos numéricos para evaluar el desempeño de pilotes Tubulares de Acero Rellenos de Concreto (CFSTP por sus siglas en inglés) embebidos, con secciones transversales circulares y cuadradas. Los resultados mostraron dos tendencias según la carga axial: $0 < P \leq 5$ MN y $P > 5$ MN. Independientemente de la relación de rigidez del suelo ($ks1/ks2 = 0.5–1.5$), el desempeño lateral estuvo dominado por la geometría, siendo el pilote cuadrado–cuadrado (SSP por sus siglas en inglés) el más eficiente, seguido del circular–circular (CCP por sus siglas en inglés) y sólido (SP por sus siglas en inglés). Los momentos flectores máximos fueron ligeramente mayores en las secciones más rígidas, particularmente SSP y CCP. Finalmente, se concluye que la carga axial provoca un efecto dual: amplificar las deflexiones laterales y reducir la variación del momento flector, demostrando que la geometría de la sección transversal es el parámetro dominante en el rendimiento del pilote.

Palabras clave

Cargas combinadas, pilotes compuestos, respuesta lateral, modelación numérica, interacción suelo–estructura.

1. INTRODUCTION

Piles are a common solution for deep foundations in structures subjected to high loads [1], [2]. In real-world scenarios, such as offshore platforms, wharves, wind turbines, bridges, port structures, and buildings on soft soils, piles do not act under isolated loads but instead experience combinations of axial, lateral, torsional, and bending moment loads [3], [4]. Studies have shown that the presence of combined loads modifies the structural response of the pile and the soil-structure interaction, requiring more complex analyses than traditional one-dimensional approaches, such as advanced numerical analyses [5].

Early studies by [6] and [7] presented approximate solutions for the problem of axially and laterally loaded piles in soil, based on experimental and analytical studies that account for the elasto–plastic nature of the soil in both cohesive and cohesionless soils. Later, [8] and [9] advanced analytical formulations to assess the nonlinear response of piles in sands and clays. The influence of axial loads on lateral response in sands and clays was investigated in detail by [10] and [11], who demonstrated through numerical models that the influence of vertical loads on the lateral response of piles depends on the sequence of applied loads, simultaneous and non-simultaneous loads, resulting in a significant increase in the capacity in sandy soils and a decrease the capacity in clayey soils.

In recent decades, numerical and experimental research has become increasingly sophisticated [12], employing three-dimensional modeling to evaluate qualitative and quantitative soil–pile interaction in clayey and sandy soils under combined loading, accounting for second-order phenomena. [13] showed that vertical loads have a slight effect on pile lateral resistance in loose sands, but significantly reduce lateral capacity in clays, making it unsafe to ignore vertical–lateral interaction; in two-layered soils, this effect depends on the properties of both the surrounding soil and the soil below the pile tip. [14] reported that soil densification governs the initial lateral loading response, while the P–Δ effect becomes dominant at higher lateral loads, causing the pile bending moment to first decrease and then increase as horizontal load grows and [15] demonstrated through experimental analysis that axial loads affect the lateral behavior and stress distribution in layered soils, with vertical loads increasing the lateral load capacity across all

pile slenderness ratios, although this effect decreases as slenderness increases, independent of pile type.

Similarly, [16] and [17] analyzed the capacity of individual piles under simultaneous torsional and axial loads through static and stability analyses. Building on these studies, [18] investigated the effects of combined vertical and torsional loads on piles embedded in layered soils, showing that pile behavior under combined loading differs from individual loading, highlighting that soil stratigraphy and load sequence strongly influence bearing performance, and indicating that the complex interaction of vertical and torsional loads must be considered in practical design.

Furthermore, [19] discussed the effects of various soil and pile-shaft properties on the dynamic response of a partially embedded single pile in unsaturated soils, founding that soil saturation strongly influences pile stiffness and dynamic response, while [20] using three-dimensional finite element analysis, evaluated the limit load of a single pile in cross-anisotropic soils under general loading, finding that soil anisotropy has a greater effect on the lateral limit load than on vertical or bending loads, while interface properties more strongly influence vertical and bending capacities than the lateral one. These findings highlight the critical role of soil conditions in the behavior of piles under combined loads, as noted by [21].

More recently, [22] analyzed Concrete-Filled Steel Tubular Piles (CFSTP) used in coastal wharf structures using finite element models under coupled horizontal-vertical and horizontal-moment loads, demonstrating their ability to redistribute internal forces through nonlinear steel-concrete interaction. Additionally, [23] and [5] experimentally examined the behavior of individual rigid piles subjected to combined axial and lateral loads, emphasizing the critical role of shaft friction, end bearing, and coupled interactions in load-bearing capacity, and the effect of soil densification using displacement visualization techniques, showing that the vertical load has a favorable effect on the lateral response of the pile in frictional soil and almost no effect on the lateral response of the pile in frictionless soil.

Currently, composite section piles, especially those composed of Concrete-Filled Steel Tubes (CFST), have proven to be an efficient and great solution for deep foundations subjected to combined loads, commonly used in port structures, bridges, and offshore platforms, although the mechanical behavior of Concrete-Filled Steel Tubular Piles (CFSTP) has been scarcely investigated [22]. This type of pile advantages the strengths of concrete (high compressive strength) and steel (high ductility and tensile strength), improving structural performance under complex loads.

Collectively, these studies have shown that simplified methods may not adequately capture the true behavior of piles, underscoring the need for advanced experimental and numerical approaches to predict pile performance under complex combined loading conditions reliably.

This study conducted a numerical analysis to investigate the influence of combined loads on pile behavior across different soil configurations and composite sections. The results showed that axial load has a dual effect: it amplifies lateral deflections while reducing the variation in bending moment, highlighting the decisive role of cross-sectional geometry and soil stiffness in pile performance. In this context, more efficient pile configurations are those associated with reduced deformation response and improved load distribution characteristics under identical loading conditions.

2. METHODOLOGY

2.1 Structural model

Figure 1a shows the schematic configuration of an embedded pile. In contrast, Figure 1b illustrates the proposed structural model, which considers the pile as a 1D Euler–Bernoulli beam-column element with generalized end-boundary conditions [24]. The beam-column element is defined as a prismatic member with linearly elastic, isotropic, and homogeneous material properties, characterized by the elastic modulus Ep, second moment of inertia Ip, cross-sectional area Ap, Poisson's ratio νp, and length L [24]. The pile is supported by an elastic

foundation defined by a modulus of subgrade reaction (i.e., Winkler parameter) that may vary with depth according to the soil profile, expressed as k(x) = ko + cx. This parameter can represent a uniform (c = 0), linear (ko = 0), or trapezoidal distribution with depth in the foundation soil [24]. The pile is subjected at the top to axial (P), lateral (Q), and moment (M) loads, while semi-rigid connections with translational and rotational stiffnesses S and κ, respectively, are considered. Shaft friction along the pile is neglected, as the model focuses on the lateral response rather than axial load transfer. The translational and rotational spring stiffnesses at ends A and B of the pile, denoted by $S_{(a,b)}$ and $\kappa_{(a,b)}$, allow the representation of classical as well as intermediate end-boundary conditions, where S = 0 and S = ∞ represent an end that is unrestrained and fully restrained in translation, and κ = 0 and κ = ∞ represent an end that is rotationally unrestrained and fully restrained, respectively [24], [25]. In addition, Figure 1c illustrates the proposed positive sign convention for the applied external loads, and Figure 1d shows the distribution of stiffness constants for the joint springs along the pile.

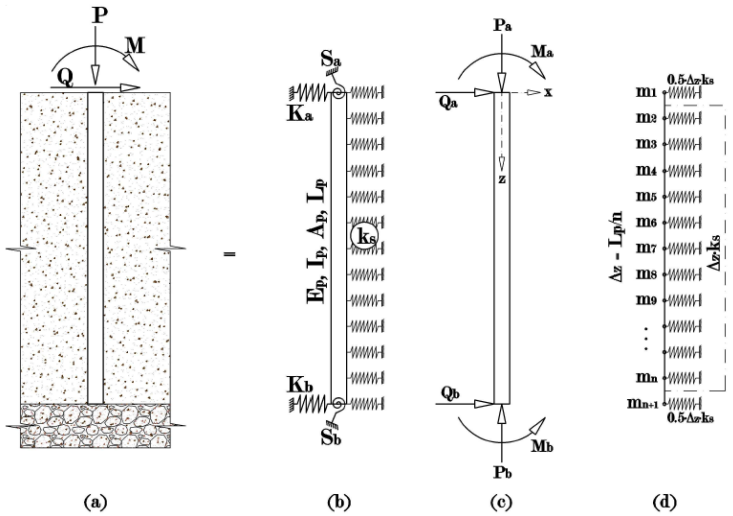


Figure 1. (a) Embedded pile scheme, (b) structural model of a pile with semi-rigid connections, (c) proposed positive sign convention for external loads, and (d) stiffness constants for joint springs. Source: adapted from [26].

This study aimed to investigate the behavior of composite piles under combined loads using numerical analysis. To achieve this objective, a comprehensive numerical modeling framework was developed using the finite–element software SAP2000, in which the pile was modeled as a beam–column element. Different pile configurations were defined to capture the effect of cross–sectional geometry on the pile response. Composite piles with solid, hollow, and circular–square steel–concrete sections were considered and modeled in SAP2000 using its built-in section designer tool, which allows defining transformed section properties and equivalent stiffness parameters, incorporating the mechanical properties of C40 concrete and S235 steel.

The soil–structure interaction was modeled using the Winkler method to simulate lateral soil resistance via linear-elastic translational elements distributed at each nodal point of the pile. Different soil profiles were analyzed, including homogeneous soil and two–layer strata, with the modulus of subgrade reaction (k_s) varied to simulate upper– and lower–layer densification. This approach allowed evaluation of the relative soil–pile stiffness ratio (k_{s1}/k_{s2}) and its influence on global pile performance.

Combined axial (P = 0, 1.25, 2.5, 5, and 10 MN) and lateral (Q = 150 kN, 300 kN, and 450 kN) loads were applied in incremental static analyses to reproduce realistic conditions of pile behavior. The analyses provided response quantities, including lateral displacement profiles, bending moment distributions, and pile base mobilization, with particular emphasis on how

axial load interacts with lateral response. To define the ultimate capacity, lateral displacement limits of 0.1D and vertical displacement limits of 0.05D were adopted. Although these limits can be conservative or not universally representative of all geotechnical scenarios, they are widely used as serviceability-based criteria in the design and analysis of pile foundations, as reported in the classical geotechnical literature and in design guidelines for pile foundations [2], [27], [28].

The finite element models were validated by comparing numerical results with analytical studies reported in the literature, ensuring the reliability of the simulations. Based on this validation, a parametric study was conducted to analyze the combined effects of cross–sectional geometry, soil–pile stiffness ratio, axial load, and soil densification. The processed results, including lateral displacements, bending moments, and effective lengths, were compared across cases and contrasted with previous findings, providing new insights into the behavior of composite piles under combined loads.

This methodological framework provides a consistent basis for investigating the behavior of composite piles subjected to combined loads through numerical analysis, enabling a systematic assessment of how sectional geometry, soil–pile relative stiffness, axial–lateral load interaction, and soil densification influence overall pile response. Validation against analytical studies strengthens the reliability of the results and contributes to advancing the understanding of composite pile behavior under complex load–soil interactions.

Figure 2 shows the pile sections employed in the finite element analysis, each with a different geometrical configuration (i.e., circular or square tubes). The specific geometric details of the piles are shown in Table 1. The materials used for all piles were concrete C40 and circular and square S235 steel tubes.

Table 1. Geometric details of the pile cross-sections used for finite element modeling. Source: own elaboration.

Section-Pile	L (m)	D_o (mm)	D_i (mm)	B_o (mm)	B_i (mm)	t_o (mm)	t_i (mm)
SP	12.5	500	---	---	---	---	---
FPP	12.5	500	---	---	---	4	---
CCP	12.5	500	250	---	---	4	4
CSP	12.5	500	---	---	250	4	4
SSP	12.5	---	---	500	250	4	4
SCP	12.5	---	250	500	---	4	4

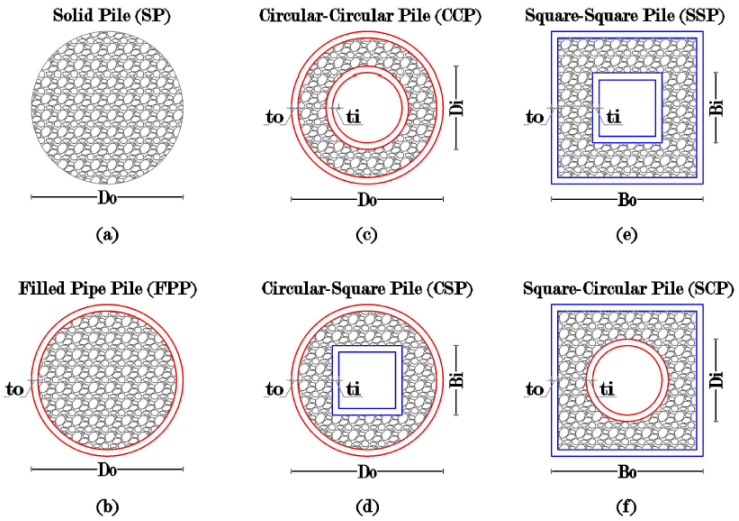


Figure 2. Different cross-section piles using circular and square tubes. Source: own elaboration.

2.2 FEM validation example

The FE model developed in SAP2000 to analyze the structural system described in the previous section was validated against the field and analytical results reported in [29] and [22], both of which involve Concrete-Filled Steel Tubular Piles (CFSTP). For the latter case, the parameters reported in [22] were adopted, with the pile having total, embedded, and rock-socketed lengths of 39.55 m, 12.55 m, and 5.2 m, respectively. The diameters in the non-rock and rock-socketed segments are 2.8 m and 2.6 m, and the exterior steel tube is 34.35 m long with a thickness of 20 mm. The soil profile comprises three layers: sand (No. 12), fully weathered rock (No. VII), and weathered rock (No. VIII). For the static analysis of the embedded length, the modulus of subgrade reaction of the soils was computed according to [16], [30], and [31], and defined as shown in (1).

$$k_s = \frac{1.3E_s}{1-\nu_s^2}\left(\frac{E_s B^4}{E_p I_p}\right)^{\frac{1}{12}} \tag{1}$$

where $E_s = 2Gs(1 + \nu s)$ and νs are the Young's modulus and Poisson ratio of the soil, respectively; B is the pile diameter; and E_pI_p is the flexural rigidity of the pile. The adopted value of ks incorporates the recommendation by [30] to double the subgrade reaction proposed by [31], accounting for the side resistance mobilized during lateral pile movement, as similarly considered by [16].

For the FEM validation example, a lateral load of Q = 285 kN and an axial load of P = 40 MN were selected. The deflection and bending moment of the pile were calculated to verify the accuracy of the results. The results from SAP2000 and those reported by [22] for lateral deflection and bending moment are shown in Figure 3 and Figure 4, respectively. The agreement between the numerical results obtained in this study and those reported in [22] was quantified by computing the average relative error. The results show an average error of 1.3% for bending moments and 0.6% for lateral deflections, confirming very good agreement between the two approaches. Hence, it could be concluded that the proposed finite element model in the present investigation is capable of modeling and capturing the performance of Concrete-Filled Steel Tubular (CFST) pile-soil interaction under a combination of axial and lateral loads.

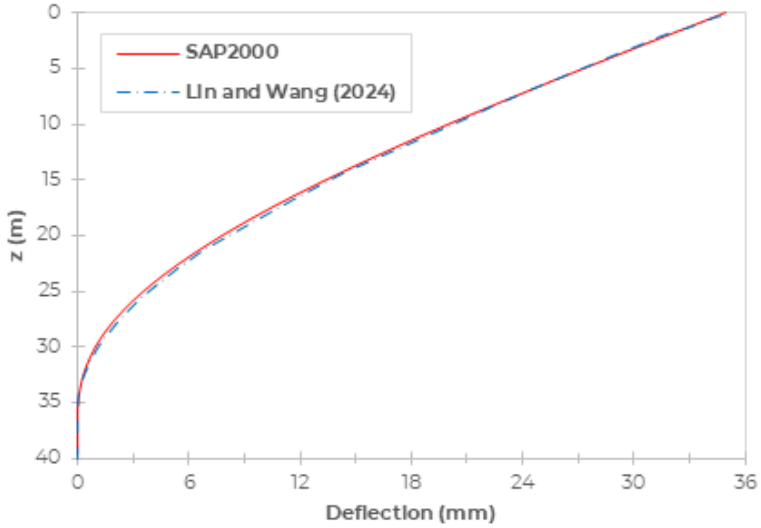


Figure 3. Lateral deflection curves of Concrete-Filled Steel Tubular Piles (CFSTP) under Q=285 kN and P=40 MN. Source: own elaboration.

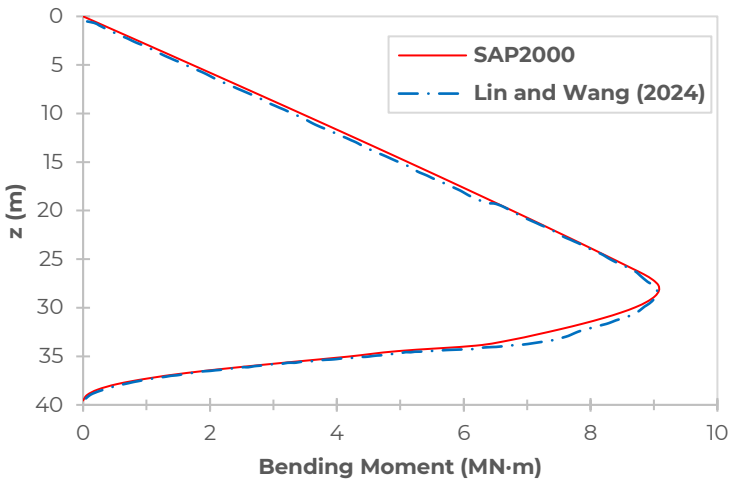


Figure 4. Bending moment curves of Concrete-Filled Steel Tubular Piles (CFSTP) under Q=285 kN and P=40 MN. Source: own elaboration.

3. RESULTS AND DISCUSSION

Three examples are presented to illustrate the behavior of various cross-section piles under combined loads. The results are analyzed to show the performance of each of them. Examples presented here aim to demonstrate the feasibility of employing different single piles with composite cross–sections to achieve comparable structural performance, providing multiple viable alternatives for addressing foundation design problems.

The pile is analyzed free at the top ($S_a = 0$, $\kappa_a = 0$) and fixed at the bottom ($S_b = \infty$, $\kappa_b = \infty$). It is assumed that the pile is made up of a linear elastic material with length L, cross-sectional area Ap, and flexural rigidity E_pI_p. For this analysis, it is assumed that the pile is filled with concrete C40 and that the inner and outer sections are made of S235 steel. In SAP2000, the element was subdivided into 50 segments to ensure high accuracy. The percentage of variation capacity (PIC) was calculated according to [10], [11], and defined as shown in (2).

$$P_{IC} = \frac{L_{CWV} - L_{CPL}}{L_{CPL}} \cdot 100 \tag{2}$$

Where L_{CWV} is the lateral load capacity with vertical load, and L_{CPL} is the lateral load capacity under pure lateral load (P = 0).

The examples analyzed and the results obtained from this investigation are presented as follows: the most relevant observations from the analyses along with a brief explanation of how these findings relate to the overall behavior of the system under study, using figures and tables. The intention is to make the results understandable and directly applicable to practical engineering situations.

3.1 Example 1: Influence of axial load on the structural behavior of piles in homogeneous soil

3.1.1 Lateral deflection of composite piles

Table 2 and Figure 5 present the maximum lateral deflection at the pile head. It can be observed that the FPP, CCP, and CSP exhibit similar behavior, and the same applies to the SSP

and SCP sections. This conclusion is supported by the fact that the differences in lateral deflection among them are less than 1%. It can also be seen that for the analyzed axial loads, two clearly identifiable increasing trends are evident. The first occurs for 0 < P ≤ 5 MN, and the second for P > 5 MN. For instance, at Q = 150 kN, the SP increases by 37.2% for 0 < P ≤ 5 MN, while for P > 5 MN, its growth rate rises to 56%. A similar trend is observed for the CCP and SSP, where for 0 < P ≤ 5 MN and P > 5 MN, their growth rates are 30.8% and 42.2%, and 20.4 and 25.6%, respectively. The same trend can also be observed for lateral loads of 300 kN. and 450 kN.

Table 2. Maximum head pile deflections under combined loads in homogeneous soil. Source: own elaboration.

Q (kN)	P (MN)	SP	FPP	CCP	CSP	SSP	SCP
		w_h (mm)					
150	0.00	13.29	12.51	12.52	12.58	11.05	11.04
	1.25	13.71	12.86	12.87	12.93	11.28	11.26
	2.50	14.16	13.22	13.24	13.30	11.53	11.51
	5.00	15.15	14.03	14.04	14.12	12.06	12.04
	10.00	17.95	16.12	16.15	16.26	13.34	13.31
300	0.00	26.58	25.02	25.04	25.15	22.11	22.08
	1.25	27.42	25.71	25.73	25.85	22.57	22.54
	2.50	28.32	26.44	26.47	26.60	23.06	23.03
	5.00	30.38	28.11	28.14	28.29	24.11	24.07
	10.00	35.90	32.37	32.41	32.64	26.68	26.63
450	0.00	39.88	37.53	37.56	37.72	33.16	33.11
	1.25	41.13	38.56	38.60	38.77	33.86	33.81
	2.50	42.47	39.67	39.70	39.90	34.59	34.54
	5.00	45.57	42.16	42.20	42.43	36.17	36.11
	10.00	53.95	48.55	48.62	48.97	40.02	39.94

Table 3 shows the percentage improvement in lateral capacity for different load combinations compared with the response under a pure lateral load (P = 0) for the six pile sections in homogeneous soil. Figure 5 indicates that, for a given lateral load, as the axial load P increases, the percentage of improvement in lateral capacity or lateral deflection among the piles becomes more pronounced. For instance, when Q = 150 kN and P increases from 0 to 10 MN, the maximum wh of the SP, CCP, and SSP increases by approximately 35, 28.9, and 20.7%, respectively. This implies that, for a given lateral load, the vertical load intensifies the lateral deformation of the piles, and the differences in lateral deformation among sections become more significant. A similar trend is observed for lateral loads of 300 kN and 450 kN, where the lateral deflection increases with the applied horizontal load and becomes more pronounced as the vertical load increases.

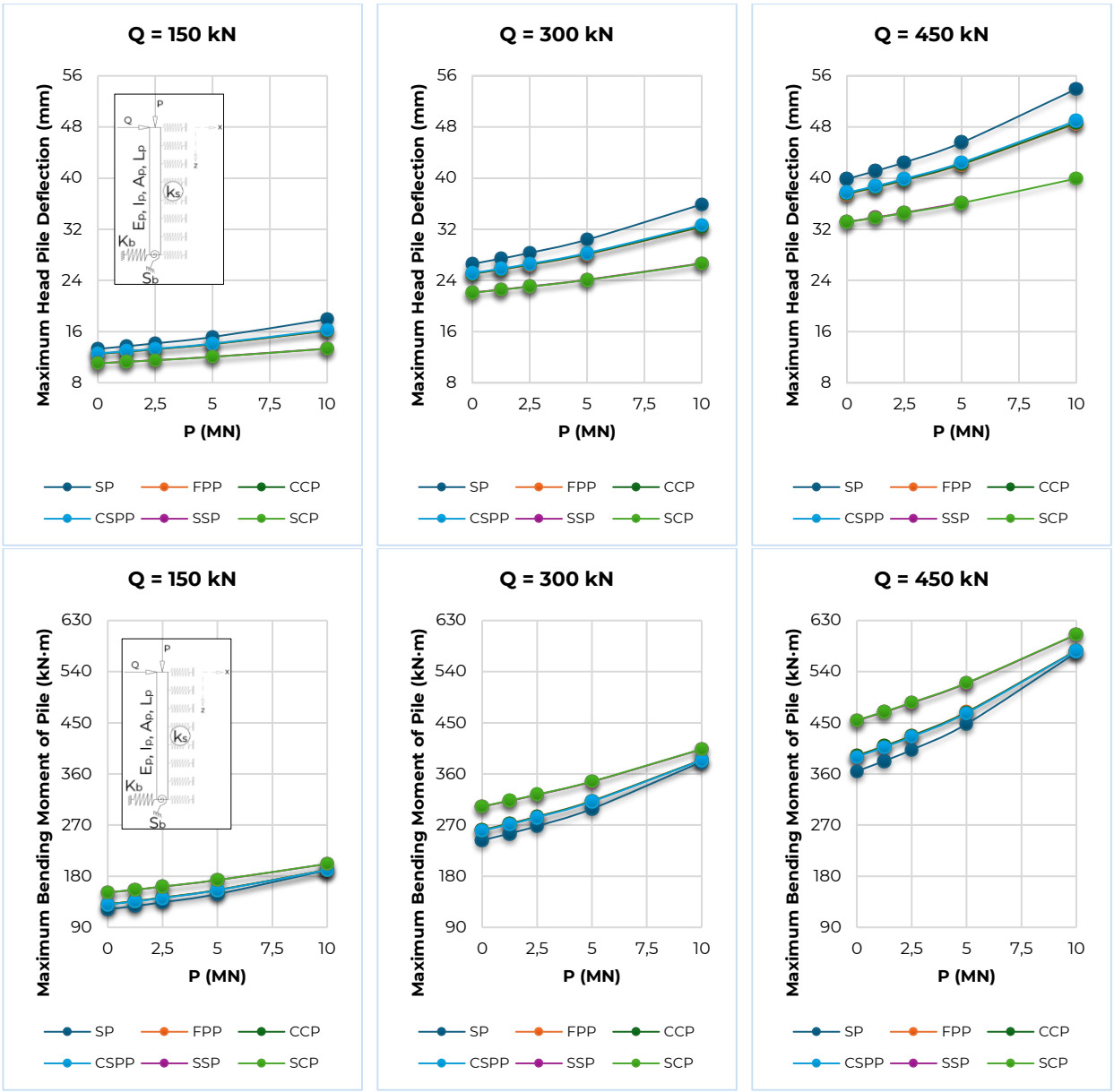


Figure 5. Variation curves of maximum lateral deflection and bending moment of composite piles under different load ratios in homogeneous soil. Source: own elaboration.

3.1.2 Bending moment along composite piles

Table 4 shows the maximum bending moment of the piles, while Table 5 presents the percentage increase for different load combinations compared to the pure lateral load case (P = 0) for the six pile sections in homogeneous soil. It is observed that under the same Q, Ma increases as P increases. For instance, when Q = 150 kN and P increases from 0 MN to 10 MN, the maximum Ma of the SP, CCP, and SSP increases by approximately 56.8%, 46.4%, and 33.3%, respectively. This implies that the presence of axial load intensifies the bending moment along the piles under lateral loading. A similar trend is observed for lateral loads of 300 kN and 450 kN, where the bending moment increases with the applied lateral load and becomes more pronounced as the vertical load increases. Therefore, Figure 5 shows that, as the axial load increases up to 10 MN, the bending moment behavior of the piles tends to converge toward similar values, especially among the SP, FPP, CCP, and CSP sections.

Table 3. Percentage of improvement in lateral capacity for head pile deflections under different load combinations in homogeneous soil. Source: own elaboration.

Q (kN)	P (MN)	SP	FPP	CCP	CSP	SSP	SCP
		P_{IC}-w_h (%)					
150	0.00	---	---	---	---	---	---
	1.25	3.1	2.8	2.8	2.8	2.1	2.0
	2.50	6.5	5.7	5.7	5.7	4.3	4.3
	5.00	14.0	12.1	12.1	12.3	9.1	9.0
	10.00	35.0	28.9	28.9	29.3	20.7	20.6
300	0.00	100.0	100.0	100.0	100.0	100.0	100.0
	1.25	106.3	105.5	105.5	105.6	104.2	104.2
	2.50	113.0	111.4	111.4	111.5	108.6	108.6
	5.00	128.6	124.7	124.7	125.0	118.2	118.1
	10.00	170.0	158.7	158.9	159.6	141.4	141.2
450	0.00	200.0	200.0	200.0	200.0	200.0	200.0
	1.25	209.4	208.3	208.3	208.3	206.3	206.3
	2.50	219.5	217.1	217.1	217.3	213.0	212.9
	5.00	242.8	237.0	237.1	237.4	227.2	227.1
	10.00	305.9	288.1	288.3	289.4	262.1	261.8

Table 4. Maximum bending moments of piles under combined loads in homogeneous soil. Source: own elaboration.

Q (kN)	P (MN)	SP	FPP	CCP	CSP	SSP	SCP
		M_a (kN·m)					
150	0.00	121.60	130.78	130.65	130.01	151.27	151.52
	1.25	127.63	136.43	136.31	135.69	156.18	156.42
	2.50	134.15	142.49	142.37	141.79	161.66	161.89
	5.00	148.67	155.83	155.73	155.23	173.19	173.40
	10.00	190.67	191.26	191.22	191.03	201.71	201.86
300	0.00	243.20	261.56	261.30	260.01	302.54	303.04
	1.25	255.25	272.86	272.61	271.38	312.65	313.13
	2.50	268.30	284.98	284.75	283.57	323.32	323.79
	5.00	298.67	312.63	312.43	311.44	346.37	346.80
	10.00	381.33	384.75	384.69	384.38	403.43	403.73
450	0.00	364.80	392.34	391.95	390.02	453.81	454.56
	1.25	382.88	409.29	408.92	407.07	468.97	469.69
	2.50	402.45	427.47	427.12	425.36	484.98	485.68
	5.00	448.00	468.94	468.64	467.16	519.56	520.20
	10.00	573.73	577.12	577.03	576.57	605.14	605.59

Table 5. Percentage of improvement in lateral capacity for bending moments under different load combinations in homogeneous soil. Source: own elaboration.

Q (kN)	P (MN)	SP	FPP	CCP	CSP	SSP	SCP
		P_{IC}-M_a (%)					
150	0.00	---	---	---	---	---	---
	1.25	5.0	4.3	4.3	4.4	3.2	3.2
	2.50	10.3	9.0	9.0	9.1	6.9	6.8
	5.00	22.3	19.2	19.2	19.4	14.5	14.4
	10.00	56.8	46.2	46.4	46.9	33.3	33.2
300	0.00	100.0	100.0	100.0	100.0	100.0	100.0
	1.25	109.9	108.6	108.7	108.7	106.7	106.7
	2.50	120.6	117.9	117.9	118.1	113.7	113.7
	5.00	145.6	139.0	139.1	139.6	129.0	128.9
	10.00	213.6	194.2	194.4	195.7	166.7	166.5
450	0.00	200.0	200.0	200.0	200.0	200.0	200.0
	1.25	214.9	213.0	213.0	213.1	210.0	210.0
	2.50	231.0	226.9	226.9	227.2	220.6	220.5
	5.00	268.4	258.6	258.7	259.3	243.5	243.3
	10.00	371.8	341.3	341.7	343.5	300.0	299.7

Figure 5 shows an inflection point at P = 5 MN, which marks two distinct response regimes. The first occurs within 0 < P ≤ 5 MN, followed by a higher increase for P > 5 MN. For example, under Q = 150 kN, the SP section exhibits a growth rate of 0.54% for 0 < P ≤ 5 MN, which rises to 0.84% beyond this threshold. A similar pattern is observed for the CCP and SSP sections, with growth rates of 0.50% and 0.71%, and 0.44% and 0.57%, respectively. The same behavior is consistently observed in Figure 5 for lateral loads of 300 kN and 450 kN.

3.2 Example 2: Influence of upper soil layer densification on the lateral response of composite piles in homogeneous two-layer soils

In order to study the influence of upper soil layer densification on the response of piles in homogeneous two–layer soils, the modulus of subgrade reaction is established as ks1 for the upper soil layer and k_{s2} for the lower soil layer. For this purpose, a k_{s1}/k_{s2} = 1.5 ratio is employed, where k_{s1} = 22.5 MN/m^3 and k_{s2} = 15 MN/m^3. The lateral deflection and bending moment of the pile are analyzed for the SP, CCP, and SSP sections under lateral loads of Q = 150 kN, 300 kN, and 450 kN, combined with axial loads of P = 0 MN, 1.25 MN, 2.5 MN, 5 MN, and 10 MN. It is assumed that the structural element has the same material and geometric properties as Example 1.

3.2.1 Lateral deflection and bending moment of composite piles

Table 6 and Figure 6 present the maximum lateral deflection at the pile head and the maximum bending moment of the pile. The results indicate that, for the axial loads considered, two distinct growth trends are consistently observed, consistent with those previously identified in Example 1. The first is for 0 < P ≤ 5 MN, and the second is for values of P > 5 MN.

Table 6. Maximum head pile deflections and bending moments under combined loads in homogeneous two-layer soil with a modulus of subgrade reaction ratio of k_{s1}/k_{s2} = 1.5. Source: own elaboration.

Q (kN)	P (MN)	SP		CCP		SSP	
		w_h (mm)	M_a (kN·m)	w_h (mm)	M_a (kN·m)	w_h (mm)	M_a (kN·m)
150	0.00	9.74	108.51	9.19	116.42	8.13	134.68
	1.25	9.98	112.68	9.39	120.36	8.27	138.23
	2.50	10.25	117.44	9.61	124.77	8.41	141.78
	5.00	10.82	127.53	10.08	134.09	8.73	150.23
	10.00	12.28	153.73	11.24	157.47	9.43	168.49
300	0.00	19.48	217.01	18.37	232.85	16.26	269.36
	1.25	19.97	225.65	18.78	240.96	16.54	276.46
	2.50	20.50	234.88	19.22	249.55	16.84	284.23
	5.00	21.67	255.70	20.16	268.17	17.46	300.46
	10.00	24.63	308.84	22.48	314.94	18.94	339.02
450	0.00	29.21	325.52	27.56	349.27	24.39	404.04
	1.25	29.96	338.48	28.17	361.43	24.81	414.94
	2.50	30.74	352.31	28.83	374.32	25.26	426.35
	5.00	32.51	383.54	30.27	402.96	26.20	450.69
	10.00	36.94	463.26	33.78	473.75	28.40	508.53

For instance, for the CCP with Q = 300 kN, when 0 < P ≤ 5 MN, the lateral deflection at the pile head increases at a rate of 35.7%, whereas for P > 5 MN, the growth rate rises to 46.5%. A comparable trend is observed for the SP and SSP sections: for 0 < P ≤ 5 MN and P > 5 MN, the corresponding growth rates are 43.9% and 59.1%, and 24.0% and 29.4%, respectively.

In terms of bending moments along the pile, for the CCP under Q = 300 kN, when 0 < P ≤ 5 MN, the bending moment increases at a rate of 0.71%, whereas for P > 5 MN, this growth rate rises to 0.94%. A comparable pattern is observed for the SP and SSP sections: for 0 < P ≤ 5 MN and P > 5 MN, the corresponding growth rates are 0.77% and 1.06%, and 0.62% and 0.77%, respectively. The same tendency is also observed for lateral loads of 150 kN and 450 kN.

Table 7 shows the percentage improvement in lateral capacity for different load combinations relative to pure lateral load (P = 0) for three pile sections in a homogeneous two–layer soil. Figure 6 shows that, for a given lateral load, as the axial load P increases, the percentage improvement in lateral capacity and lateral deflection among the piles tends to be more pronounced. For instance, when Q = 300 kN and P increases from 0 to 10 MN, the maximum wh of the SP, CCP, and SSP increases by approximately 52.9 %, 44.8 %, and 32.9 %, respectively. Under the same conditions, when Q = 300 kN and P increases from 0 MN to 10 MN, the maximum Ma of the SP, CCP, and SSP increases by approximately 84.6%, 70.5%, and 51.7%, respectively.

The above implies that, for a given lateral load, the vertical load aggravates the lateral deformation and bending moment of the piles. However, Figure 6 shows that when the axial loads increase up to 10 MN: i) the difference in lateral deformation between sections becomes greater, and ii) the bending moments tend to converge toward the same value, especially between the SP and CCP sections A similar trend is observed for lateral loads of 150 kN and 450 kN, where both the lateral deflection and bending moment increase with the applied horizontal load and become more pronounced as the vertical load increases.

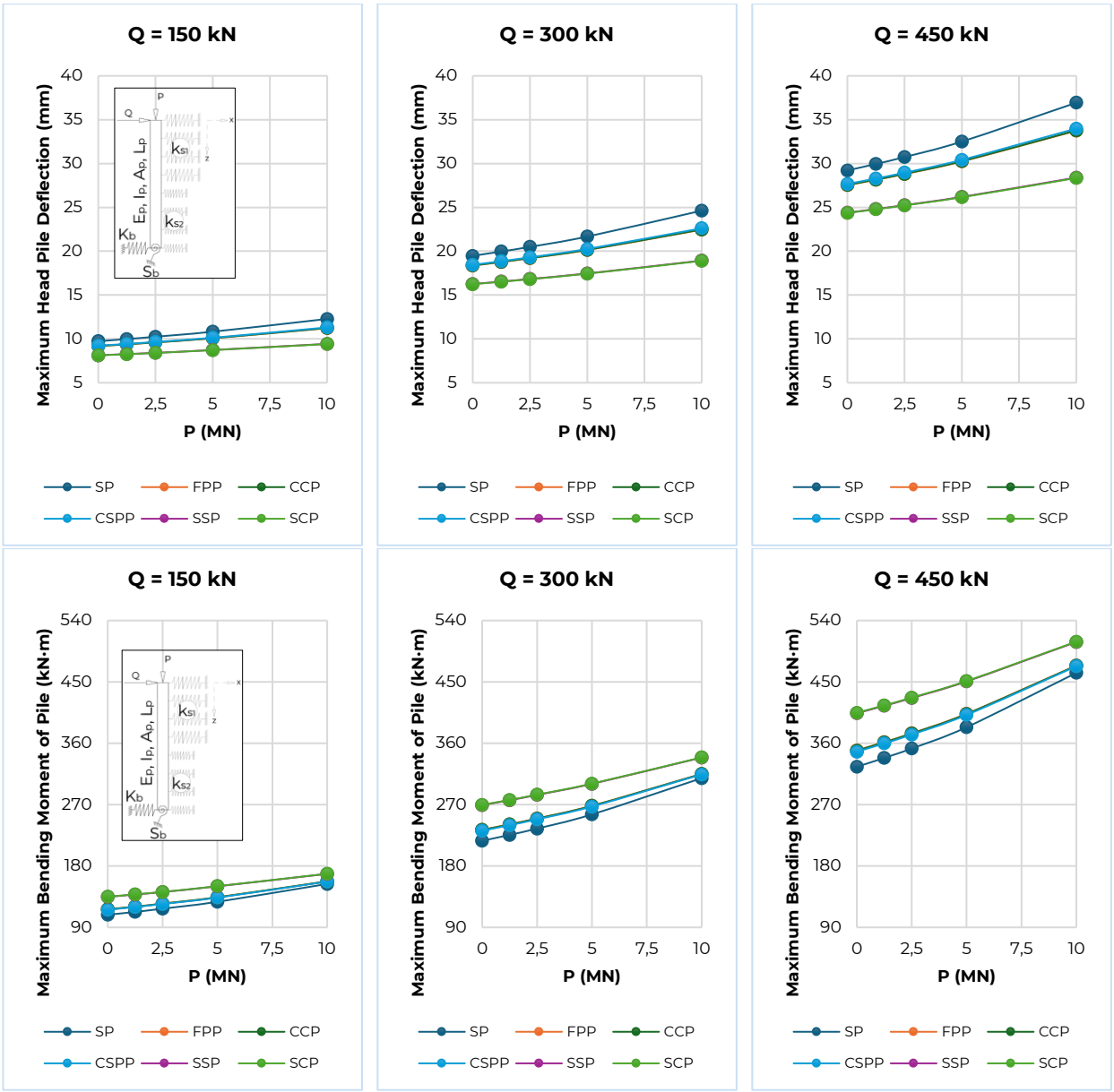


Figure 6. Variation curves of maximum lateral deflection and bending moment of composite piles under different load ratios in homogeneous two-layer soil with modulus of subgrade reaction ratio of k_{s1}/k_{s2} = 1.5. Source: own elaboration.

3.2.2 Lateral response of composite piles in homogeneous two-layer soils under the influence of the soil reaction modulus ratio ks1/ks2 = 1 and ks1/ks2 = 1.5

A higher subgrade reaction modulus in the upper soil layer provides greater resistance to the pile's lateral response. The influence of the upper boundary conditions on the horizontal response is particularly significant. In contrast, the effect of the axial load is notably reduced as the subgrade reaction modulus increases, thereby enhancing the lateral bearing capacity of the pile.

A detailed comparison of the results obtained for lateral deformation and bending moments is presented below for the SP, CCP, and SSP sections. The analysis considers two soil reaction modulus ratios, k_{s1}/k_{s2} = 1 and 1.5, to highlight the influence of soil stiffness on the pile's lateral response.

Table 7. Percentage of improvement in lateral capacity for head pile deflections and bending moments under different load combinations in homogeneous two-layer soil with a modulus of subgrade reaction ratio of k_{s1}/k_{s2} = 1.5. Source: own elaboration.

Q (kN)	P (MN)	SP		CCP		SSP	
		w_h (%)	M_a (%)	w_h (%)	M_a (%)	w_h (%)	M_a (%)
150	0.00	---	---	---	---	---	---
	1.25	2.5	3.8	2.2	3.4	1.7	2.6
	2.50	5.2	8.2	4.6	7.2	3.4	5.3
	5.00	11.1	17.5	9.7	15.2	7.4	11.5
	10.00	26.1	41.7	22.4	35.3	16.0	25.1
300	0.00	100.0	100.0	100.0	100.0	100.0	100.0
	1.25	105.1	108.0	104.5	107.0	103.4	105.3
	2.50	110.5	116.5	109.2	114.3	107.1	111.0
	5.00	122.5	135.7	119.5	130.3	114.8	123.1
	10.00	152.9	184.6	144.8	170.5	132.9	151.7
450	0.00	200.0	200.0	200.0	200.0	200.0	200.0
	1.25	207.6	211.9	206.7	210.4	205.2	208.1
	2.50	215.7	224.7	213.8	221.5	210.7	216.6
	5.00	233.8	253.5	229.5	246.1	222.2	234.6
	10.00	279.3	326.9	267.8	306.9	249.4	277.6

In the case of SP, when the soil reaction modulus ratio k_{s1}/k_{s2} = 1, the maximum head pile deflection under Q = 150 kN and P = 0 was calculated as 13.29 mm. In contrast, for the same pile section under the same load and soil conditions (k_{s1}/k_{s2} = 1.5), the maximum head pile deflection was calculated as 9.74 mm, resulting in a decrease of 36.4%.

In relation to the above, for k_{s1}/k_{s2} = 1, when the vertical load increased from 0 to 10 MN, the maximum lateral deflection increased to 17.95 mm, corresponding to a 35% increase. Under the same conditions, but with k_{s1}/k_{s2} = 1.5, the percentage increase was reduced to 26.1%, resulting in a maximum lateral deflection of 12.28 mm. A comparison of these results indicates that increasing the soil reaction modulus ratio from k_{s1}/k_{s2} = 1 to 1.5 reduced the lateral deflection of the head pile by 46.2%.

Regarding the bending moment for SP, when the soil reaction modulus ratio k_{s1}/k_{s2} = 1, under Q = 150 kN and P = 0, it was calculated as 121.60 kN·m, whereas for the same pile section under the same load and soil conditions (k_{s1}/k_{s2} = 1.5), the maximum bending moment was calculated as 108.51 kN·m, resulting in a decrease of 12.1%.

Moreover, for k_{s1}/k_{s2} = 1, when the vertical load increased from 0 MN to 10 MN, the maximum bending moment along the pile reached 190.67 kN·m, corresponding to an increase of 56.8%. Under the same conditions, but with k_{s1}/k_{s2} = 1.5, the percentage increase was reduced to 41.7%, resulting in a maximum bending moment along the pile of 153.73 kN·m. A comparison of these results indicates that increasing the soil reaction modulus ratio from k_{s1}/k_{s2} = 1 to 1.5 reduced the bending moment along the pile by 24%.

A similar trend is observed for CCP and SSP with lateral loads of 300 kN and 450 kN, where the lateral deflection and bending moment values are greater for k_{s1}/k_{s2} = 1 than for k_{s1}/k_{s2} = 1.5 under combined loads.

3.3 Example 3: Influence of lower soil layer densification on the lateral response of composite piles in homogeneous two-layer soils

To investigate the influence of densification of the lower soil layer on the response of piles in homogeneous two–layer soils, the modulus of subgrade reaction is defined as in Example 2, with k_{s1} assigned to the upper soil layer and k_{s2} to the lower soil layer. For this analysis, a ratio of $k_{s1}/k_{s2} = 0.5$ is adopted, with $k_{s1} = 15$ MN/m^3 and $k_{s2} = 30$ MN/m^3. Lateral deflection and bending moment of the pile are analyzed for SP, CCP, and SSP sections under lateral loads of Q = 150, 300, and 450 kN in combination with axial loads of P = 0 MN, 1.25 MN, 2.5 MN, 5 MN, and 10 MN. It is assumed that the structural element has the same material and geometric properties as those of Example 1.

3.3.1 Lateral deflection and bending moment of composite piles

Table 8 and Figure 7 present the maximum lateral deflection of the head pile and the maximum bending moment of the pile. The results indicate that, for the axial loads considered, two distinct growth trends are consistently maintained, in line with those previously identified in Examples 1 and 2. The first trend is for $0 < P \leq 5$ MN, and the second is for values of $P > 5$ MN.

For instance, for the SSP with Q = 450 kN, when $0 < P \leq 5$ MN, the lateral deflection at the pile head increases at a rate of 58.3%, whereas for $P > 5$ MN, this rate rises to 73.7%. This behavior reflects a progressive amplification of lateral deformation as the axial load increases beyond the initial range. A similar pattern is observed for the SP and CCP sections, for $0 < P \leq 5$ MN and $P > 5$ MN, the corresponding growth rates are 110.5% and 160.8%, and 89.7% and 122.5%, respectively, indicating that sections with lower flexural stiffness experience more pronounced deformations under combined loading.

Table 8. Maximum head pile deflections and bending moments under combined loads in homogeneous two-layer soil with a modulus of subgrade reaction ratio of $k_{s1}/k_{s2} = 0.5$
Source: own elaboration.

Q (kN)	P (MN)	SP		CCP		SSP	
		w_h (mm)	M_a (kN·m)	w_h (mm)	M_a (kN·m)	w_h (mm)	M_a (kN·m)
150	0.00	13.24	122.31	12.47	131.31	11.02	151.65
	1.25	13.64	128.38	12.80	136.99	11.24	156.55
	2.50	14.08	134.93	13.16	143.07	11.48	162.00
	5.00	15.04	149.51	13.94	156.44	11.99	173.46
	10.00	17.72	191.35	15.95	191.72	13.22	201.59
300	0.00	26.47	244.62	24.93	262.62	22.03	303.30
	1.25	27.28	256.75	25.60	273.97	22.48	313.38
	2.50	28.15	269.86	26.31	286.13	22.96	324.01
	5.00	30.15	300.31	27.92	313.80	23.98	346.91
	10.00	35.45	382.69	32.00	385.53	26.43	403.19
450	0.00	39.70	366.93	37.40	393.92	33.05	454.96
	1.25	40.92	385.13	38.40	410.96	33.73	470.07
	2.50	42.23	404.79	39.47	429.20	34.44	486.01
	5.00	45.23	450.46	41.88	470.70	35.96	520.37
	10.00	53.27	575.65	48.00	578.30	39.65	604.78

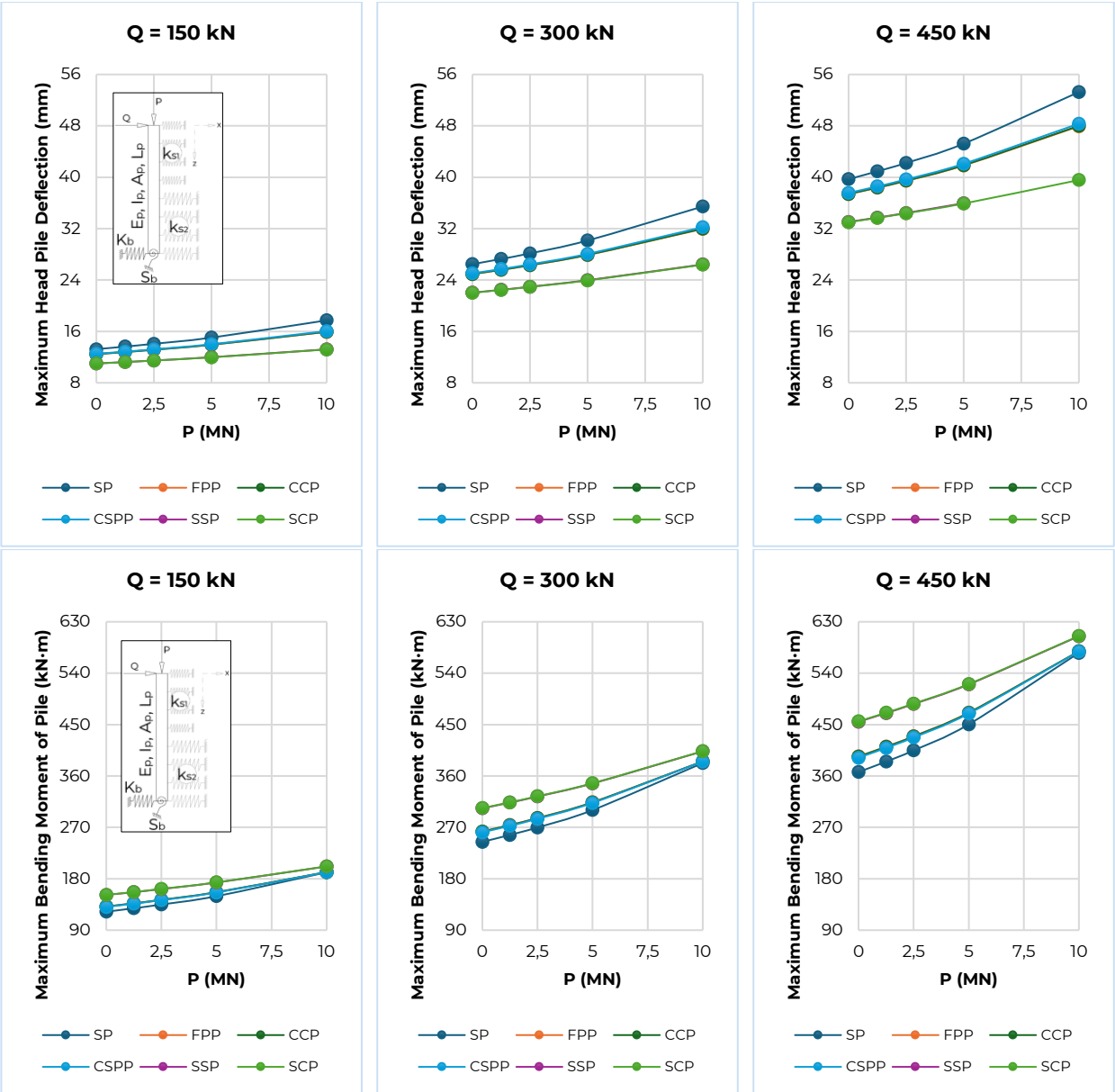


Figure 7. Variation curves of maximum lateral deflection and bending moment of composite piles under different load ratios in homogeneous two-layer soil with modulus of subgrade reaction ratio of k_{s1}/k_{s2} = 0.5. Source: own elaboration.

In terms of bending moments along the pile, under Q = 450 kN for the SSP, when 0 < P ≤ 5 MN, the bending moment increases at 1.31%, and for P > 5 MN, this growth rate increases to 1.69%. A comparable trend is also observed for the SP and CCP: for 0 < P ≤ 5 MN and P > 5 MN, their growth rates are 1.67% and 2.50%, and 1.54% and 2.15%, respectively. These results confirm that, as the axial load increases, the bending moments not only grow but also show a nonlinear amplification consistent with the P–Δ effects discussed earlier. The same overall trend is observed in Figure6 for lateral loads of 150 kN and 300 kN.

Table 9 shows the percentage of improvement in lateral capacity for different load combinations compared with that under pure lateral load (P = 0) for three-section piles in homogeneous two–layer soil. Figure 7 shows that, for a given lateral load, when the axial load P increases, the percentage of improvement in lateral capacity of lateral deflection between the piles tends to be more pronounced. For instance, when Q = 450 kN and P increases from 0

to 10 MN, the maximum wh of the SP, CCP, and SSP would be increased by approximately 102.5%, 85.1%, and 59.9%, respectively. Under the same conditions, when Q = 450 kN and P increases from 0 to 10 MN, the maximum Ma of the SP, CCP, and SSP would be increased by approximately 170.7 %, 140.4 %, and 98.8 %, respectively.

Table 9. Percentage of improvement in lateral capacity for head pile deflections and bending moments under different load combinations in homogeneous two-layer soil with a modulus of subgrade reaction ratio of k_{s1}/k_{s2} = 0.5. Source: own elaboration.

Q (kN)	P (MN)	SP		CCP		SSP	
		w_h (%)	M_a (%)	w_h (%)	M_a (%)	w_h (%)	M_a (%)
150	0.00	---	---	---	---	---	---
	1.25	3.1	5.0	2.7	4.3	2.0	3.2
	2.50	6.4	10.3	5.6	9.0	4.2	6.8
	5.00	13.6	22.2	11.8	19.1	8.8	14.4
	10.00	33.9	56.4	27.9	46.0	20.0	32.9
300	0.00	100.0	100.0	100.0	100.0	100.0	100.0
	1.25	106.1	109.9	105.4	108.6	104.1	106.6
	2.50	112.7	120.6	111.1	117.9	108.4	113.7
	5.00	127.8	145.5	124.0	139.0	117.6	128.8
	10.00	167.8	212.9	156.7	193.6	139.9	165.9
450	0.00	200.0	200.0	200.0	200.0	200.0	200.0
	1.25	209.2	214.9	208.1	213.0	206.1	210.0
	2.50	219.1	231.0	216.7	226.9	212.6	220.5
	5.00	241.7	268.3	236.0	258.5	226.5	243.1
	10.00	302.5	370.7	285.1	340.4	259.9	298.8

The above implies that, for a given lateral load, the vertical load aggravates the lateral deformation and bending moment of the piles. However, Figure 7 shows that, when the axial loads increase up to 10 MN: i) the difference in lateral deformation between sections becomes greater, and ii) bending moments tend to converge toward the same value, especially between the sections SP and CCP. A similar trend is observed for the lateral loads of 150 kN and 300 kN, where the lateral deflection and bending moment increase with the applied horizontal load and become more pronounced as the vertical load increases.

From Tables 2, 4, and 8, and by comparing the results for maximum lateral deflection and bending moment of the pile under the same axial and lateral load conditions in Examples 1 and 3, where k_{s1}/k_{s2} = 1 and k_{s1}/k_{s2} = 0.5, respectively, it can be observed that the densification of the lower stratum in Example 3 does not significantly affect the behavior of the pile. To illustrate the above, for the CCP section under Q = 150 kN and P = 0, with k_{s1}/k_{s2} = 1, the maximum lateral deflection increased from 12.52 mm to 16.15 mm as the vertical load rose from 0 MN to 10 MN, corresponding to a 28.9% increase. Under the same conditions, but with k_{s1}/k_{s2} = 0.5, the maximum lateral deflection increased from 12.47 mm to 15.95 mm, reflecting a 27.9% increase and a difference of only 1.2% between the two cases. Regarding the bending moment, for CCP with k_{s1}/k_{s2} = 1, the maximum value under Q = 150 kN and P = 0 was 130.65 kN·m, while for k_{s1}/k_{s2} = 0.5 it was 131.31 kN·m, yielding a difference of less than 0.5%.

3.4 Discussion

The results of the analysis of composite-section piles reveal an intermediate behavior between solid and hollow cross-sections, balancing stiffness, and flexibility. The findings show that the SSP (high flexural stiffness) exhibits lower deflections but higher bending moments,

whereas the SP (solid section, lower stiffness) displays the opposite trend. Similar behavior was observed by [32], who reported that as soil–pile relative stiffness increases, normalized lateral load-displacement curves present reduced displacements under the same loads, while bending moment profiles become more concentrated, reflecting a stiffer response.

The variation in pile–soil relative stiffness and its effects shows that increasing k_{s1}/k_{s2} (i.e., densifying the upper soil layer) produces a substantial reduction in lateral deflections with only moderate increases in bending moments. In contrast, lowering the ratio (i.e., densifying the lower layer) yields much smaller improvements. These findings are consistent with those of [33], who reported that the bending moment increases with the lateral soil displacement and the displacement at the soil surface also increases with the axial load, and that pile–soil relative stiffness governs horizontal displacement and strongly influences bending moment behavior, turning out to be the main influencing factor.

With increasing axial load, two distinct trends can be observed in lateral deflections and bending moments, with moderate increases up to certain load thresholds, beyond which the response accelerates due to second-order (P–Δ) effects; similar findings were reported by [12]. This type of nonlinearity under increased axial load was also observed by [34], who reported that maximum bending moments and displacements increase with axial load and lateral soil movement, indicating that lateral deformation is strongly influenced by the level of axial load, particularly when lateral soil movement is significant. Similarly, [35], in their study on prestressed high-strength concrete piles, found that bending capacity increases with axial force up to a point, after which ductility decreases, and deformations amplify rapidly once the load ratio exceeds a threshold. Similar findings were also reported by [36] and [37].

Regarding the influence of section stiffness, sections with greater moments of inertia (e.g., SSP) exhibit a stiffer response but concentrate curvature and bending moment near the base. This aligns with the observations of [33], who reported that relative pile–soil stiffness is the primary factor governing pile horizontal displacement, with the dominant influence arising from soil resistance at the pile toe, resulting in smaller top displacements but higher bending moment demands. Similarly, [38] indicated that as lateral loads increase, stiffer piles develop higher bending moments at critical sections more rapidly, while displacements remain relatively small; in general, maximum lateral displacement and bending moment increase with higher vertical and lateral loads but decrease with increasing pile stiffness and subgrade reaction coefficient.

This numerical analysis show that the performance of composite–section piles depend on their relative stiffness, the soil–pile interaction, and the applied loading conditions, thereby making the proposed methodology appropriate for preliminary analysis and parametric evaluation of pile behavior, particularly for assessing the influence of cross-sectional configurations on structural performance. In actual geotechnical practice, this means designers can strategically adapt the stiffness of piles and soil improvements to achieve the desired results in terms of serviceability and strength. For example, increasing the stiffness of the upper layer or selecting sections with higher moments of inertia can substantially reduce lateral deflections, but at the cost of higher bending moments that must be compensated for by reinforcements or section capacity. Similarly, using more flexible sections or improving the deeper layers yields diminishing returns and may not sufficiently limit lateral movement. The observed trends toward moderate to accelerated growth in deflections and moments under higher axial loads highlight the importance of accounting for P–Δ effects in foundations subjected to complex loads, particularly in large–scale pile–supported structures.

4. CONCLUSIONS

Based on this numerical analysis, the following conclusions can be drawn.

The results from Examples 1, 2, and 3 show that cross-sectional geometry has a major influence on pile behavior under combined loading. The SSP developed smaller lateral

displacements but higher bending moments, as its square section with double confinement provides a much larger moment of inertia than the other configurations. This higher flexural stiffness (E_pI_p) effectively restrains lateral movement and reduces pile-head displacements. At the same time, the increased stiffness leads to a concentration of curvature in critical zones, particularly near the pile base, rather than a more uniform distribution along the shaft. As a result, larger peak bending moments are observed, indicating a stiffer but more demanding structural response. Overall, the SSP showed performance comparable to that of the SCP.

The SP, despite being fully solid, exhibits lower bending moments and larger lateral displacements due to its relatively lower flexural stiffness (E_pI_p) and the absence of additional confinement. Its smaller effective moment of inertia provides less resistance to lateral curvature, resulting in greater pile-head deflections under identical loading conditions. However, the induced curvature tends to be distributed over a larger portion of the shaft, which reduces stress concentration near the pile base. Consequently, peak bending moments are lower than those in stiffer sections, although with a more flexible and less efficient lateral response. The CCP exhibits intermediate behavior between the SP and the SSP. Due to the circular geometry, which promotes a more uniform stress distribution, the CCP shows a balanced structural performance, similar to that observed for the CSP and FPP.

Based on Examples 1, 2, and 3, two almost linear trends are observed, the first for axial loads $0 < P \leq 5$MN and the second for $P > 5$ MN, both associated with gradual increases in lateral displacement and bending moment. When the axial load increases up to 10 MN, the response curves exhibit two clear tendencies: i) the difference in lateral deformation between sections increases, while ii) bending moments tend to approach similar values due to P–Δ effects, which lead to a rapid growth of lateral deflections and bending moments. These results demonstrate that axial load not only amplifies lateral deflections but also reduces the variation of bending moment demand across different pile cross-sections. This dual effect underscores the importance of considering both the load magnitude and the cross-sectional geometry when evaluating pile performance under combined loads.

The study shows that soil stratigraphy affects pile response in an asymmetric influence. Higher stiffness in the upper soil layer significantly reduces lateral displacements and enhances load transfer, whereas greater stiffness in the lower layer provides only limited improvement. This highlights the relevance of the stiffness ratio k_{s1}/k_{s2}. Composite piles, due to their higher stiffness and confinement, are more effective at exploiting improved soil conditions and provide greater bending capacity and ductility than conventional sections, underscoring the need to consider both geotechnical and structural factors in lateral performance.

5. ACKNOWLEDGMENTS

This research was carried out at the University of Antioquia in Medellín, Colombia. The support and suggestions of the Infrastructure Research Group (GII) of the University of Antioquia are appreciated. This research did not receive any specific financial support.

6. REFERENCES

[1] B. M. Das, *Principles of foundation engineering*, 9th ed. Boston, MA, USA: Cengage Learning, 2019. https://pdfcoffee.com/principles-of-foundation-engineering-9th-edition-si-edition-by-braja-m-das-nagaratnam-sivakugan-pdf-free.html

[2] M. J. Tomlinson, and J. Woodward, *Pile design and construction practice*, 6th ed. Boca Raton, FL, USA: CRC Press, 2015. https://books.google.com.co/books/about/Pile_Design_and_Construction_Practice_Si.html?id=Me2sBAAAQBAJ&redir_esc=y

[3] L. C. Reese, *Single Piles And Pile Groups Under Lateral Loading*. Boca Raton, FL, USA: CRC Press, 2026. https://books.google.com.co/books?id=buTqBgAAQBAJ&printsec=frontcover&redir_esc=y#v=onepage&q&f=false

[4] D. P. Coduto, W. A., Kitch, and M. R. Yeung, *Foundation Design: Principles And Practices*, 3rd ed. Boston, MA, USA: Pearson, 2016. https://books.google.com.co/books/about/Foundation_Design.html?id=m9C_oQEACAAJ&redir_esc=y

[5] S. S. Al-Amery, and M. H. Al-Dahlaki, "Behavior of Piles Subjected to Combined Axial and Lateral Loading," *Eng. Technol. Appl. Sci. Res.*, vol. 15, no. 2, pp. 21187-21196, Apr. 2025. https://doi.org/10.48084/etasr.9798

[6] A. J. Valsangkar, N. S. V. Kameswara Rao, and P. K. Basudhar, "Generalized Solutions of Axially and Laterally Loaded Piles in Elasto–Plastic Soil," *Soils Found.*, vol. 13, no. 4, pp. 1-14, Dec. 1973. https://doi.org/10.3208/sandf1972.13.4_1

[7] B. F. Goryunov, "Analysis of piles subjected to the combined action of vertical and horizontal loads (discussion)," *Soil Mech. Found. Eng.*, vol. 10, no. 1, pp. 10-13, Jan. 1973. https://doi.org/10.1007/BF01706631

[8] Y.-M. Hsiung, S.-S. Chen, and Y.-C. Chou, "Analytical Solution for Piles Supporting Combined Lateral Loads," *J. Geotech. Geoenvironmental Eng.*, vol. 132, no. 10, pp. 1315-1324, Oct. 2006. https://doi.org/10.1061/(ASCE)1090-0241(2006)132:10(1315)

[9] M. Achmus, and K. Thieken, "On The Behavior of Piles in Non-Cohesive Soil Under Combined Horizontal and Vertical Loading," *Acta Geotech.*, vol. 5, pp. 199-210, Sep. 2010. https://doi.org/10.1007/s11440-010-0124-1

[10] S. Karthigeyan, V. V. G. S. T. Ramakrishna, and K. Rajagopal, "Influence of Vertical Load on the Lateral Response of Piles in Sand," *Comput. Geotech.*, vol. 33, no. 2, pp. 121-131, Mar. 2006. https://doi.org/10.1016/j.compgeo.2005.12.002

[11] S. Karthigeyan, V. V. G. S. T. Ramakrishna, and K. Rajagopal, "Numerical Investigation of the Effect of Vertical Load on the Lateral Response of Piles," *J. Geotech. Geoenvironmental Eng.*, vol. 133, no. 5, pp. 512-521, May. 2007. https://doi.org/10.1061/(ASCE)1090-0241(2007)133:5(512)

[12] T. E. Zormpa, and E. M. Comodromos, "Numerical Evaluation of Pile Response Under Combined Lateral and Axial Loading," *Geotech. Geol. Eng.*, vol. 36, no. 2, pp. 793-811, Apr. 2017. https://doi.org/10.1007/s10706-017-0354-1

[13] L. Hazzar, M. N. Hussien, and M. Karray, "Influence of Vertical Loads on Lateral Response of Pile Foundations in Sands and Clays," *J. Rock Mech. Geotech. Eng.*, vol. 9, no. 2, pp. 291-304, Apr. 2017. https://doi.org/10.1016/j.jrmge.2016.09.002

[14] W. Lu, and G. Zhang, "Influence Mechanism of Vertical-Horizontal combined loads on the Response of a Single Pile in Sand," *Soils Found.*, vol. 58, no. 5, pp. 1228-1239, Oct. 2018. https://doi.org/10.1016/j.sandf.2018.07.002

[15] S. Farhan Ibrahim, M. S. Al-Soud, and F. I. Al-Asadi, "Performance of A Single Pile Under Combined Axial and Lateral Loads in Layered Sandy Soil," *J. Eng. Sustain. Dev.*, vol. 22, no. 1, pp. 121-136, Jan. 2018. https://jeasd.uomustansiriyah.edu.iq/index.php/jeasd/article/view/329

[16] C. A. Vega-Posada, A. P. Gallant, and M. Areiza-Hurtado, "Simple approach for analysis of beam-column elements on homogeneous and non-homogeneous elastic soil," *Eng. Struct.*, vol. 221, p. 111110, Oct. 2020. https://doi.org/10.1016/j.engstruct.2020.111110

[17] S.-W. Wang, J. Jiang, C.-Z. Fu, X.-D. Ou, and J. Tang, "Analysis of the Bearing Characteristics of Single Piles Under Vertical and Torsional Combined Loads," *Adv. Civ. Eng.*, vol. 2021, p. 8896673, Feb. 2021. https://doi.org/10.1155/2021/8896673

[18] X. Zou, C. Zhou, X. Cao, and Y. Wang, "Experimental Studies on the Behaviour of Single Pile Under Combined Vertical-Torsional Loads in Layered Soil," *Appl. Ocean Res.*, vol. 106, p. 102457, Jan. 2021. https://doi.org/10.1016/j.apor.2020.102457

[19] X. Zou, Z. Yang, and W. Wu, "Horizontal Dynamic Response of Partially Embedded Single Pile in Unsaturated Soil Under Combined Loads," *Soil Dyn. Earthq. Eng.*, vol. 165, p. 107672, Feb. 2023. https://doi.org/10.1016/j.soildyn.2022.107672

[20] A. Izadi, and R. Jamshidi Chenari, "Combined Load Bearing Capacity of Rigid Piles Embedded in a Cross-Anisotropic Clay Deposit Using 3D Finite Element Lower Bound," *J. Rock Mech. Geotech. Eng.*, vol. 15, no. 3, pp. 717-737, Mar. 2023. https://doi.org/10.1016/j.jrmge.2022.05.012

[21] Q. Li, L. J. Prendergast, A. Askarinejad, and K. Gavin, "Influence of Vertical Loading on Behavior of Laterally Loaded Foundation Piles: A Review," *J. Mar. Sci. Eng.*, vol. 8, no. 12, p. 1029, Dec. 2020. https://doi.org/10.3390/jmse8121029

[22] L. Lin, and F. Wang, "Analytical Behavior of Concrete-Filled Steel Tubular Pile Used in Coastal Wharf Structure Subjected to Combined Loads," *Ocean Eng.*, vol. 308, p. 118388, Sep. 2024. https://doi.org/10.1016/j.oceaneng.2024.118388

[23] F. Zhang, G. Dai, X. Li, F. Xu, and W. Gong, "Numerical Solution for the Laterally Loaded Rigid Piles Considering Resisting Force and Moment Under Combined Loadings," *Ocean Eng.*, vol. 292, p. 116225, Jan. 2024. https://doi.org/10.1016/j.oceaneng.2023.116225

[24] C. A. Vega-Posada, D. G. Zapata-Medina, and E. F. Garcia Aristizabal, "Analytical Formulation for the study of the effect of shear deformations on beam-columns and piles: engesser and haringx theories," *Soils Found.*, vol. 64, no. 3, p. 101446, Jun. 2024. https://doi.org/10.1016/j.sandf.2024.101446

[25] J. D. Aristizabal-Ochoa, "First- and Second-Order Stiffness Matrices and Load Vector of Beam-Columns with Semirigid Connections," *J. Struct. Eng.*, vol. 123, no. 5, pp. 669-678, May. 1997. https://doi.org/10.1061/(ASCE)0733-9445(1997)123:5(669)

[26] C. J. Fernández-Escobar, C. A. Vega-Posada, and E. F. Garcia-Aristizábal, "Lateral deformation and buckling analysis of piles including shear effects: Numerical analysis," *Eng. Struct.*, vol. 277, p. 115416, Feb. 2023. https://doi.org/10.1016/j.engstruct.2022.115416

[27] API Recommended Practice 2A-WSD: Planning, Designing, and Constructing Fixed Offshore Platforms – Working Stress Design, 21th ed., American Petroleum Institute, API, Washington, USA, 2014. [Online]. Available: https://es.scribd.com/document/211447689/2Ati

[28] Geotechnical and foundation design considerations, API RP 2GEO, American Petroleum Institute, Washington, USA, 2011, p. 120. https://standards.globalspec.com/std/9878475/api-rp-2geo

[29] J.-J. Chen, J.-H. Wang, X. Ke, and D.-S. Jeng, "Behavior of Large-Diameter Rock-Socketed Piles Under Lateral Loads," *Int. J. Offshore Polar Eng.*, vol. 21, no. 04, Dec. 2011. https://onepetro.org/IJOPE/article-abstract/35572/Behavior-of-Large-Diameter-Rock-Socketed-Piles?redirectedFrom=fulltext

[30] J. E. Bowles, and Y. Guo, *Foundation Analysis and Design*, 5th ed., vol. 5. New York, USA: McGraw-hill, 1997. https://www.u-cursos.cl/ingenieria/2012/1/CI4402/1/material_docente/detalle?id=424204

[31] A. B. Vesić, "Bending of Beams Resting on Isotropic Elastic Solid," *J. Eng. Mech. Div.*, vol. 87, no. 2, pp. 35-53, Apr. 1961. https://doi.org/10.1061/JMCEA3.0000212

[32] B. Liu, X. Wang, C. Liu, and J. Kong, "Effect of Relative Stiffness of Pile and Soil on Pile Group Effect," *J. Mar. Sci. Eng.*, vol. 11, no. 1, p. 192, Jan. 2023. https://doi.org/10.3390/jmse11010192

[33] B. Yuan, M. Chen, W. Chen, Q. Luo, and H. Li, "Effect of Pile-Soil Relative Stiffness on Deformation Characteristics of the Laterally Loaded Pile," *Adv. Mater. Sci. Eng.*, vol. 2022, no. 1, p. 4913887, May. 2022. https://doi.org/10.1155/2022/4913887

[34] Z. Feng Zhang, and J. Pei Li, "Analysis of Piles Subject to Axial Load and Lateral Soil Movement," *Adv. Mater. Res.*, vol. 383, pp. 1708-1713, Nov. 2011. https://doi.org/10.4028/www.scientific.net/AMR.383-390.1708

[35] Z. Yang, G. Li, W. Wang, and Y. Lv, "Study on the Flexural Performance of Prestressed High Strength Concrete Pile," *KSCE J. Civ. Eng.*, vol. 22, no. 10, pp. 4073-4082, Oct. 2018. https://doi.org/10.1007/s12205-018-1811-y

[36] J. Han, and J. D. Frost, "Load–Deflection Response of Transversely Isotropic Piles Under Lateral Loads," *Int. J. Numer. Anal. Methods Geomech.*, vol. 24, no. 5, pp. 509-529, Apr. 2000. https://doi.org/10.1002/(SICI)1096-9853(20000425)24:5%3C509::AID-NAG79%3E3.0.CO;2-9

[37] L. Zhang, X. Gong, Z. Yang, and J. Yu, "Elastoplastic solutions for single piles under combined vertical and lateral loads," *J. Cent. South Univ. Technol.*, vol. 18, no. 1, pp. 216-222, Feb. 2011. https://doi.org/https://doi.org/10.1007/s11771-011-0682-x

[38] C. Feng *et al.*, "Mechanical Property of Lateral Piles for Pile Composite Foundation Loaded by Model Test," *Adv. Civ. Eng.*, vol. 2023, no. 1, p. 6538496, Apr. 2023. https://doi.org/10.1155/2023/6538496

CONFLICT OF INTEREST

The authors declare that they have no known competing financial interests or personal relationships that could have appeared to influence the work reported in this article.

AUTHORSHIP CONTRIBUTION

Alejandro Nasner-Caipe: Methodology, Software, Writing – original draft.
Carlos Alberto Vega-Posada: Conceptualization, Methodology, Software, Writing – original and final draft preparation.
Edwin Garcia-Aristizábal: Writing – review and editing, and final drafts.

AI DECLARATION

During the preparation of this work, the authors used Grammarly PRO to improve the manuscript's readability and language. After using this tool, the authors reviewed and edited the content as needed and take full responsibility for the published article.